

PAPER • OPEN ACCESS

# Selection of silicon photomultipliers for a ${}^6\text{LiF:ZnS(Ag)}$ scintillator based cold neutron detector

To cite this article: A Osovizky *et al* 2018 *J. Phys. Commun.* **2** 045009

View the [article online](#) for updates and enhancements.

## Related content

- [Energy resolution of small scintillation detectors with SiPM light readout](#)  
M Grodzicka, M Moszynski, T Szczniak et al.
- [Characterization of blue sensitive  \$3 \times 3 \text{ mm}^2\$  SiPMs and their use in PET](#)  
F R Schneider, T R Ganka, G eker et al.
- [Silicon photomultipliers for high energy physics detectors](#)  
Erika Garutti



## PAPER

Selection of silicon photomultipliers for a  ${}^6\text{LiF:ZnS(Ag)}$  scintillator based cold neutron detector

## OPEN ACCESS

## RECEIVED

16 October 2017

## REVISED

14 February 2018

## ACCEPTED FOR PUBLICATION

2 March 2018

## PUBLISHED

4 April 2018

Original content from this work may be used under the terms of the [Creative Commons Attribution 3.0 licence](#).

Any further distribution of this work must maintain attribution to the author(s) and the title of the work, journal citation and DOI.



A Osovizky<sup>1,2,4</sup>, K Pritchard<sup>1</sup>, Y Yehuda-Zada<sup>3</sup>, J B Ziegler<sup>1</sup>, P Tsai<sup>1</sup>, M Ghelman<sup>3</sup>, A K Thompson<sup>1</sup>, R M Ibberson<sup>1</sup>, G M Baltic<sup>1</sup>, C F Majkrzak<sup>1</sup> and N C Maliszewskyj<sup>1</sup>

<sup>1</sup> NIST Center for Neutron Research, Gaithersburg, Maryland, the United States of America

<sup>2</sup> Rotem Industries Ltd, Rotem Industrial Park, Israel

<sup>3</sup> Nuclear Research Center Negev, Beer-Sheva Israel

<sup>4</sup> University of Maryland, College Park, Maryland, the United States of America

E-mail: [nicholas.maliszewskyj@nist.gov](mailto:nicholas.maliszewskyj@nist.gov)

**Keywords:** SiPM, neutron detector,  ${}^6\text{LiF:ZnS(Ag)}$ , CANDoR, gamma rejection

### Abstract

We describe the process of selecting a silicon photomultiplier (SiPM) as the light sensor for an ultrathin ( $\approx 2$  mm) highly efficient cold neutron detector. The neutron detector consists of  ${}^6\text{LiF:ZnS(Ag)}$  scintillator in which wavelength shifting (WLS) fibers have been embedded. The WLS fibers conduct the scintillation light out from the scintillator to the SiPM photosensor. In addition to the many benefits of using silicon photomultipliers as photosensors (low cost, compact size, insensitivity to magnetic fields), their selection also presents many challenges (thermally induced dark noise, delayed cross talk, afterpulsing, etc) which are not shared by traditional photomultiplier tubes. In this work, we discuss the considerations for the selection of the appropriate silicon photomultiplier to achieve the best net neutron sensitivity and gamma ray discrimination. Important characteristics for these devices include short recovery time ( $\approx 35$  ns), high photodetection efficiency ( $> 30\%$  at the target wavelength), low thermal noise ( $< 35$  kHz  $\text{mm}^{-2}$  at ambient temperatures), and low crosstalk.

### Introduction

Neutrons are an effective tool to probe the structure of materials [1]. More specifically, neutron diffraction can be applied to determine the atomic and magnetic structure of materials. Collimated beams of thermal or cold neutrons diffract from the specimen and the direction, energy, and intensity of the scattered neutrons contain information about the structure of that material.

A recent project at the NIST Center for Neutron Research (NCNR) is the development of the Chromatic Analysis Neutron Diffractometer or Reflectometer (CANDoR) [2]. Unlike conventional instruments at continuous sources which use a monochromatic neutron beam and detect neutrons elastically scattered from the sample, CANDoR will use a polychromatic incident beam and will energy analyze the scattered radiation. This will be accomplished using a linear array of pyrolytic graphic crystals set at successively increasing takeoff angles which Bragg-diffract neutrons entering the array into corresponding detectors lining the sides of the array. This design is intended to permit CANDoR to measure a typical reflectometry curve an order of magnitude faster than a reflectometer employing a single monochromatic beam. If the neutron detector is exceedingly thin ( $\approx 2$  mm) many such energy analyzing arrays can be packed closely together to measure scattering in several scattering angles simultaneously.

To meet the spatial constraints of the instrument design, the CANDoR neutron detector consists of slabs of neutron sensitive scintillator which have been pressed around an array of Kuraray Y-11 wavelength shifting [3] (WLS) fibers. The WLS fibers conduct the scintillation light out of the plane of the scintillator to the photosensor (figure 1). Outside of the slab, the fibers are concentrated into a 3 mm  $\times$  3 mm bundle mating with a SiPM [4] [5].

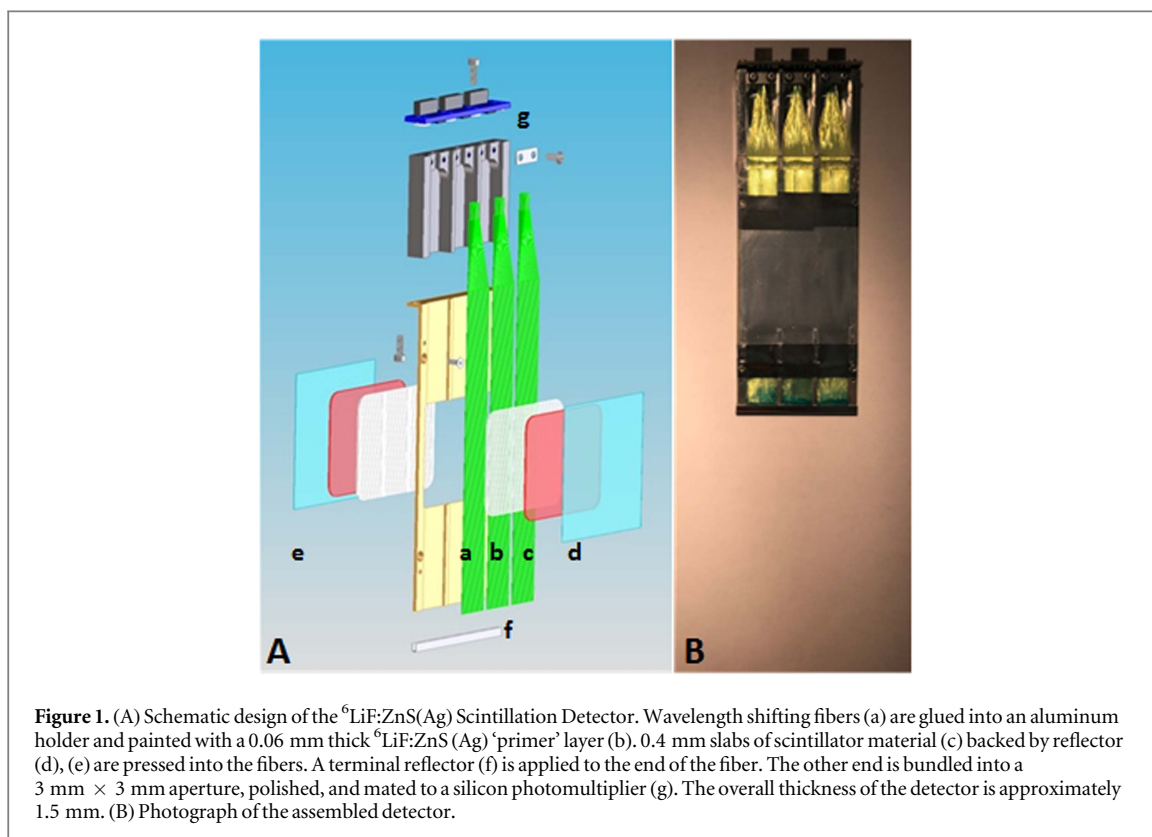


**Figure 1.** (A) Schematic design of the  ${}^6\text{LiF:ZnS(Ag)}$  Scintillation Detector. Wavelength shifting fibers (a) are glued into an aluminum holder and painted with a 0.06 mm thick  ${}^6\text{LiF:ZnS(Ag)}$  'primer' layer (b). 0.4 mm slabs of scintillator material (c) backed by reflector (d), (e) are pressed into the fibers. A terminal reflector (f) is applied to the end of the fiber. The other end is bundled into a 3 mm  $\times$  3 mm aperture, polished, and mated to a silicon photomultiplier (g). The overall thickness of the detector is approximately 1.5 mm. (B) Photograph of the assembled detector.

Several other research groups have built position sensitive neutron detectors using sheets of scintillator with WLS fiber readout [6, 7]. Another group has built a thermal neutron counter using the same scintillator with a mechanically embedded wavelength shifting fiber read out with an SiPM [8]. To our knowledge no other group has been motivated to build a detector with thinness being a primary constraint [9].

The  ${}^6\text{LiF:ZnS(Ag)}$  scintillator slab [10] can be represented by three principal components:  ${}^6\text{LiF}$  salt with a high  ${}^6\text{Li}$  number density, a  $\text{ZnS(Ag)}$  phosphor with a high light yield, and an organic binder for combining the two powders and improving light transmission in the medium. In a neutron capture reaction, alpha and triton particles are produced with high Q value  ${}^6\text{Li}+n \rightarrow \text{Triton (2.74 MeV)} + \text{Alpha (2.06 MeV)}$  [11–13]. These particles ionize the  $\text{ZnS(Ag)}$  and produce light. It is estimated that about 160 000 photons are produced per neutron capture [14]. Those blue light photons emitted by the  $\text{ZnS(Ag)}$  reach the WLS fibers and are absorbed by the K-27 fluorescent dye and are re-emitted as green photons. About 5 percent of the green photons are transmitted by the fiber to the photosensor where again the number is reduced because of the imperfect photodetection efficiency of the device.

### Silicon photomultiplier

The silicon photomultiplier (SiPM) is a solid state optical sensor based on an array of avalanche photodiodes (APDs) operating in a Geiger-mode [15]. The appealing properties of the SiPM, principally low cost, radiation hardness [16, 17], insensitivity to magnetic fields, and compact size make it of particular interest for our application. Other researchers have employed them in neutron detection applications as well [8, 18, 19]. Advances in the design of these devices have resulted in improvements in photon detection efficiency (PDE) from 20% to 30% and a reduction of the dark noise rate from 1 MHz events per  $\text{mm}^2$  to less than 30 kHz per  $\text{mm}^2$ . Low dark noise could permit operating the devices with higher bias voltages which improve the PDE without considerably increasing the dark noise to a level that interferes with neutron discrimination. Additionally, it is important to note that operating these devices at uncontrolled ambient temperatures may present challenges due to the thermal dependence of both gain and breakdown voltage.

The principal challenge of using the SiPM in our application is the discrimination of neutron capture events from gamma capture or thermal noise events. Since the amplitude of neutron and gamma ray events can be similar, pulse height techniques are insufficient to distinguish the two. Pulse shape discrimination techniques, however, are much more effective.

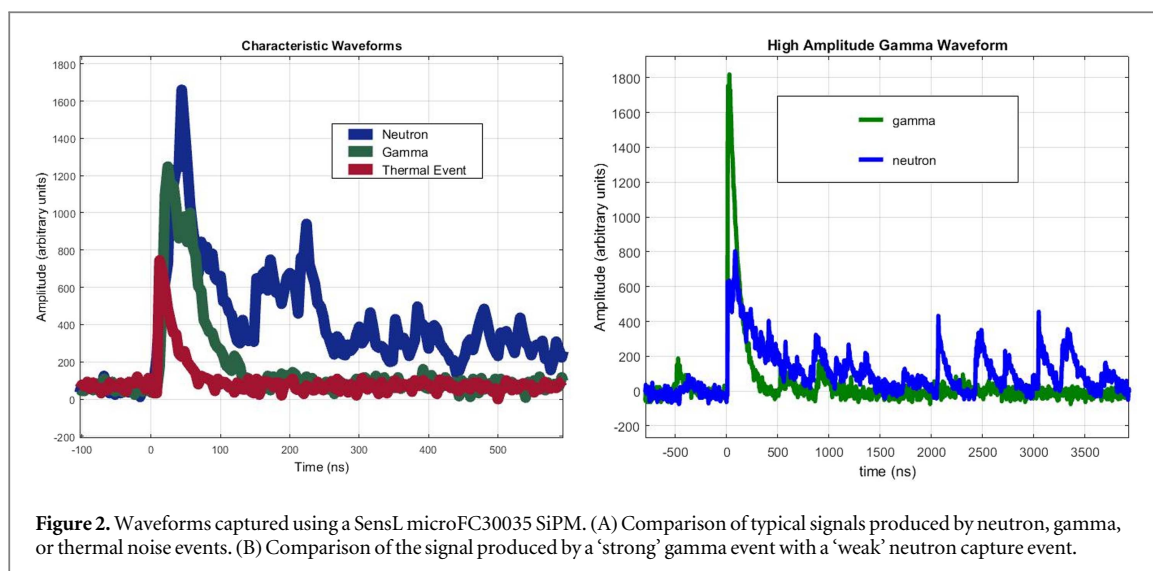


**Figure 2.** Waveforms captured using a SensL microFC30035 SiPM. (A) Comparison of typical signals produced by neutron, gamma, or thermal noise events. (B) Comparison of the signal produced by a ‘strong’ gamma event with a ‘weak’ neutron capture event.

Figure 2(a) shows typical waveforms obtained using a Hamamatsu S12572 MPPC (multipixel photon counter) [20]. This device has a fast recovery time, on the order of 25 ns. As can be seen from the figure, gamma ray and thermal noise events typically decay in less than 100 ns. Neutron events tend to persist longer than 200 ns [21–24]. If the intrinsic optical signal from the scintillator is broadened by a convolution with the electrical response of the SiPM, it can become much more complicated to discriminate the desired neutron events from other types. Additionally, it is also clear that the neutron event tail (the later period of the decay) can also be utilized for discrimination between signal and noise. In figure 2(b) it is clear that the gamma event has a higher amplitude than the neutron event, and that the strength of the signal in the tail region can be used as a tool for discriminating between the two event types. However, if the signal from the neutron event is weak, the signal in the tail is correspondingly small and it becomes much harder to use the tail integration as the principal discrimination parameter. To maintain good gamma rejection ( $\approx 10^{-7}$ ) it will be necessary to sacrifice some neutron sensitivity.

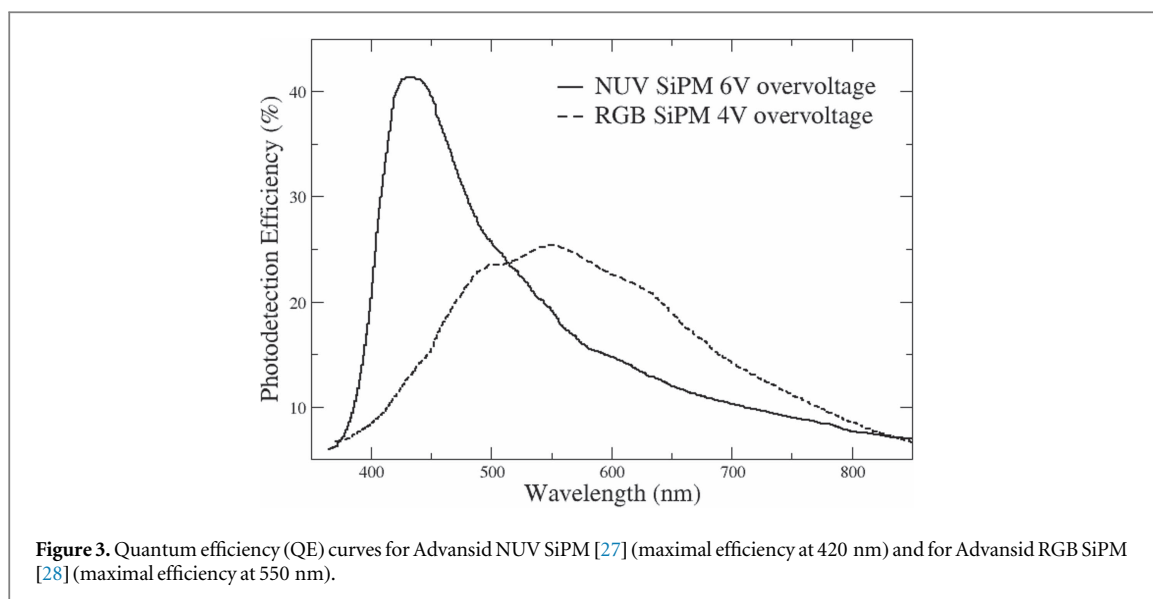
Disadvantages of using the SiPM as the photosensor include thermal noise and afterpulsing [25, 26]. Afterpulsing creates a correlated delay response (self-firing) of some of the pixels which could, in combination with the true photon flux and the thermal noise, present an output signal that masquerades as a marginally detectable neutron event.

## Experimental

Measurements involving neutrons were performed at the NG1 detector test station at the NIST Center for Neutron Research. Beryllium-filtered neutrons (to remove wavelengths shorter than approximately 4 Å) moderated by a liquid hydrogen cold source at the NBSR at NIST incident on the scintillator were monochromated to 4.75 Å (3.62 meV) using the (002) atomic planes of pyrolytic graphite and masked to form a spot of approximately 0.6 cm in diameter. The fractional wavelength resolution was of the order of 1% and the horizontal and vertical angular divergences of the incident beam were of the order of several minutes of arc and a few degrees, respectively.

For gamma rejection measurements we used isotopic  $^{137}\text{Cs}$  and  $^{60}\text{Co}$  sources of known activity placed directly on the scintillator in the absence of neutrons (reactor off). We counted the number of candidate neutron events passed through by the pulse shape discriminator per hour and divided by half the source activity (to correct for the solid angle subtended by the detector) over the same period to determine the gamma rejection ratio. Typical values for this quantity were determined to be  $\approx 2 \times 10^{-7}$ .

The signal chain, post SiPM, consisted of a bias source and preamplifier followed by a high speed digitizer. The preamplifier has a rise time of 40 ns, a bandwidth of 25 MHz, and a gain of  $5 \text{ V mA}^{-1}$ . The typical waveform amplitude before the digitizer was 200 mV. Waveforms were captured using a Picoscope 3206B digital oscilloscope. Real time neutron event discrimination was accomplished using a 4DSP FMC104 4-channel  $250 \text{ MS s}^{-1}$  analog to digital converter with a Xilinx Virtex 6 field programmable gate array processing the incoming signal.



## Photosensor selection

Proper selection of the SiPM should focus on enhancing the signal and reducing dark noise to optimize the detection sensitivity and provide a clean signal for pulse shape discrimination. The principal parameters for evaluation of the SiPM are:

### Photon detection efficiency (PDE)

The PDE is set by three parameters: the geometrical efficiency (GE), the quantum efficiency of the light photon wavelength (QE), and the probability for inducing an avalanche. It is desirable to increase the SiPM PDE to enhance light collection. This will increase the likelihood of detecting neutron events with lower light production. With higher PDE, the neutron signal tail will be detected even for low light yield neutron events by presenting a cleaner raw signal for pulse shape discrimination.

### Geometric efficiency (GE)

The GE determines the probability of a light photon reaching an active diode surface. Part of the diode surface includes conductors from the pixels and these dead zones reduce the PDE. The geometrical efficiency can partly be adjusted for optimization by the user by selecting the pixel size. Typically, a device with a smaller pixel size has more 'dead' area associated with the boundaries between cells. The pixel size affects the device dynamic range (energy resolution). In our application, the dynamic range of the device has a negligible effect because the resolution required for discrimination between the neutron signal and the noise can be achieved with all devices.

### Geiger mode avalanche

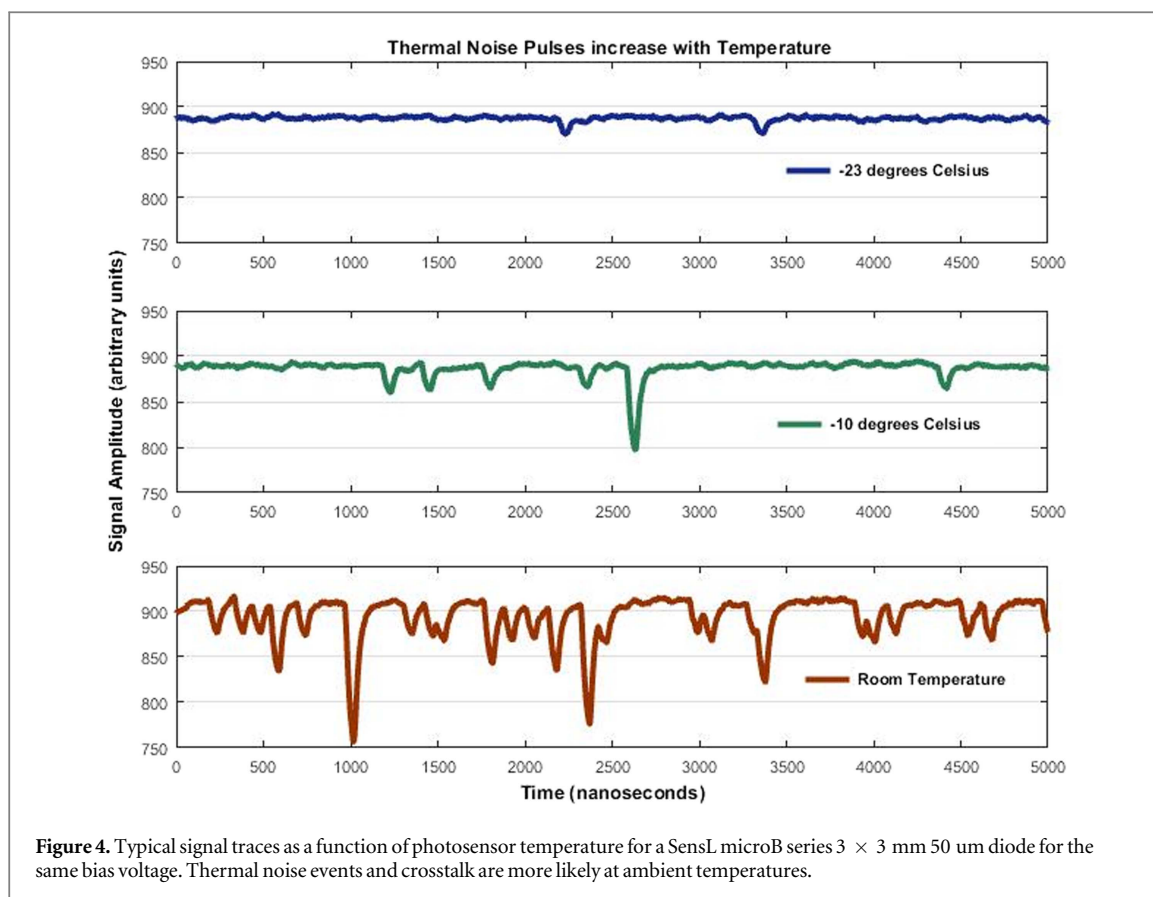
The probability for firing each pixel and inducing the avalanche can be improved by applying a higher bias voltage to the diode. This, however, also increases the frequency of thermal noise. For SensL 'C' series SiPMs, the PDE can be improved by 30% when a bias voltage higher than breakdown voltage is applied (31% @2.5 V versus 41% @5 V). The dark current frequency doubles at higher bias voltage (300 kHz @2.5 V versus 600 kHz @5 V). Hence an educated selection needs to be made based on the pulse integration time.

### Quantum efficiency (QE)

The QE is the SiPM sensitivity as a function of the interacting light photon wavelength (see figure 3). Devices can be optimized for peak sensitivity (green, blue or red light photons). The best overlap is obtained by matching the SiPM peak QE to the peak transmission wavelength emission of the light (in our design 476 nm of the WLS fiber).

### Stable breakdown voltage

In a batch of SiPMs operating at the same temperature, there is variation between the actual breakdown voltage of each individual device. For a system that is based on more than 1600 sensors (as employed in the CANDoR instrument), this variation presents a challenge during the calibration process as the applied overvoltage for a



common bias voltage varies. This variation can result in a different gain for each channel and therefore a different signal amplitude requiring a unique discrimination level (calibration) for each detector.

### Crosstalk

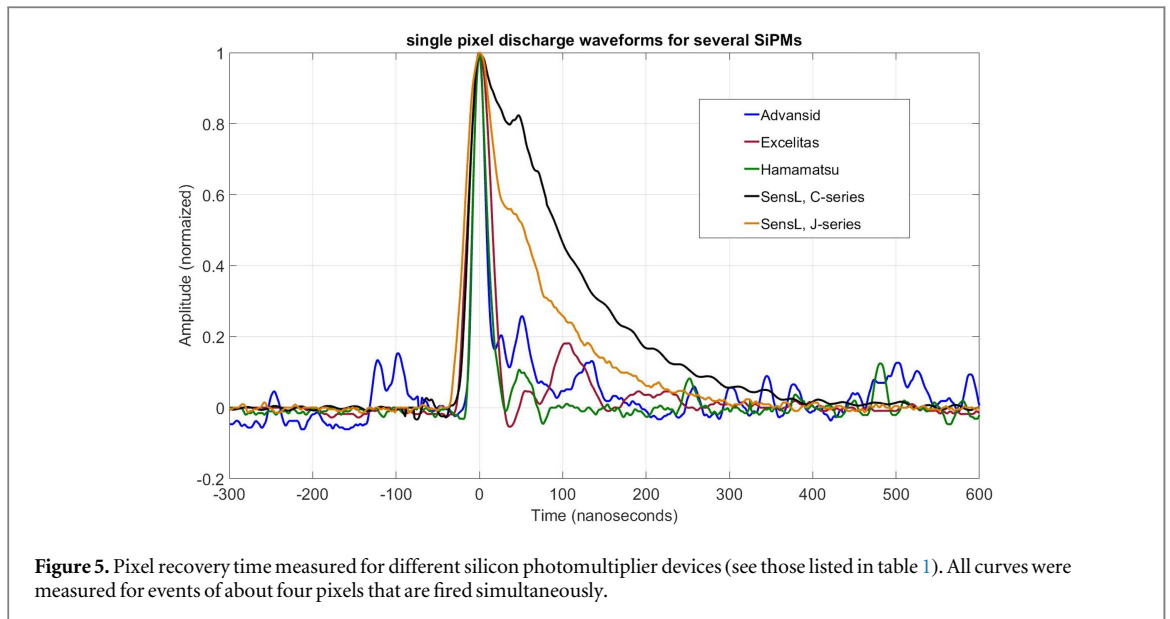
Crosstalk causes multiple pixels to be fired by a single light photon. Typically, its impact is on the amplitude of thermal events and a high enough amplitude could cross the threshold for triggering the neutron detection process. Another important parameter for our application is the probability of delayed crosstalk ('afterpulsing'). Although the probability for afterpulsing is low, it is a very important parameter since the delayed events causing pixels to be fired with a correlated delay from the original burst of light could be incorrectly determined to be a neutron capture event. The probability for cross talk and the delayed cross talk increases when a higher overvoltage is applied. For the Hamamatsu S12571 the probability for crosstalk increases from 2.5% at the recommended 2.5 V overvoltage to more than 10% at 5 V overvoltage.

### Dark noise

High thermal noise makes it much harder to distinguish between the tail of a neutron capture signal and intrinsic background. For older series of devices (e.g. SensL B series [29]), 10 or more pixels could fire in a period of one microsecond so active cooling is required to decrease the frequency of thermally induced noise spikes. Newer devices (e.g. SensL C [30] and J series [31]) have dark count rates lower than one event per  $\mu$ s and can therefore be operated at ambient temperatures even at high bias voltages. In all cases, the signal to noise ratio of the device is improved by cooling it. The optimal operating temperature is that which reduces the dark current to the point where only a single pixel will self-fire over the duration of the measurement. The dark noise can be reduced by factor of 50 when the working temperature is reduced from ambient temperature to  $-25$  °C [32, 33] (figure 4) while the scintillator light output is constant over this temperature range [34]. An additional benefit of active cooling is that it stabilizes the temperature, preventing fluctuations in the breakdown voltage which in turn result in fluctuations in gain.

### Recovery time

For a pulse shape discrimination algorithm, short recovery times are preferred to minimize the thermal noise pulse width with respect to the intrinsic decay time of the scintillator crystal. The recovery time is typically shorter for devices with a smaller pixel size, but devices with smaller pixel size have lower overall PDE. The



recovery time curve measured for five different silicon photomultiplier devices with the same surface area of  $3 \text{ mm} \times 3 \text{ mm}$  is presented in figure 5. The gain was normalized for receiving similar amplitudes for events corresponding to the firing of four pixels simultaneously.

### Diode dimensions

Dark current is proportional to the active area of the diode. The active area should ideally be only minimally larger than the area of the fiber bundle.

In table 1 we compare several candidate devices we evaluated based on the properties which are most germane to our application (QE matched to the WLS fiber emission wavelength, high PDE, short recovery time, low dark noise, and low crosstalk). None of the devices we investigated was optimal in all respects (the best values are highlighted in bold).

A simulation was performed to evaluate the tradeoff between the parameters for the gamma discrimination. We determined that similar sensitivity can be obtained using either devices with high PDE and long recovery time or those with lower PDE and short recovery time.

The data in figures 6 and 7 are simulations of the time dependence of neutron and gamma capture events as measured by SiPMs with different characteristics. In these simulations we used integrated amplitudes of 5000 photons for a gamma capture event and 500 photons for a neutron capture event. The formula was a simple decaying exponential. The intrinsic decay time constant for the gamma event was set to be 50 ns. For neutron capture events we used two time constants: 100 ns for the first 150 ns and 250 ns for the remainder of the event. These decay time constants were selected to simulate the light decay curves obtained from gamma and neutron events (as presented in figure 2). These values are similar to what we have measured empirically with a traditional photomultiplier with negligible recovery time. We have selected the probability of delayed cross talk to be about 3% and compared two devices with two recovery times of 50 ns and 200 ns. The data was analyzed once without statistical fluctuations and once with fluctuations of two standard deviations to emphasize the effect when a high gamma rejection is required. The noise level was estimated at an amplitude of ten light photons.

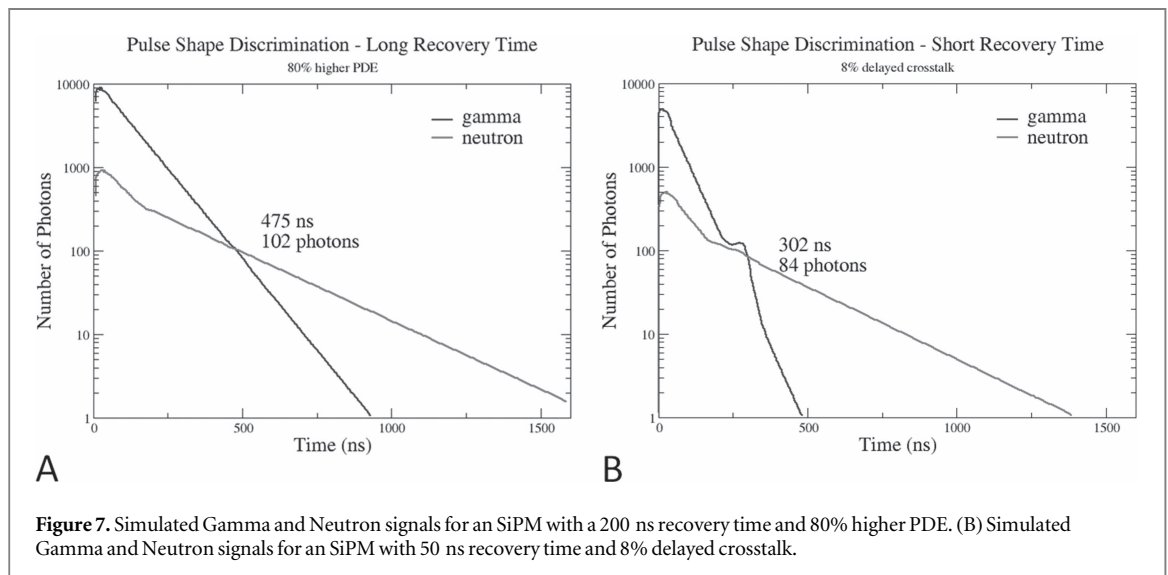
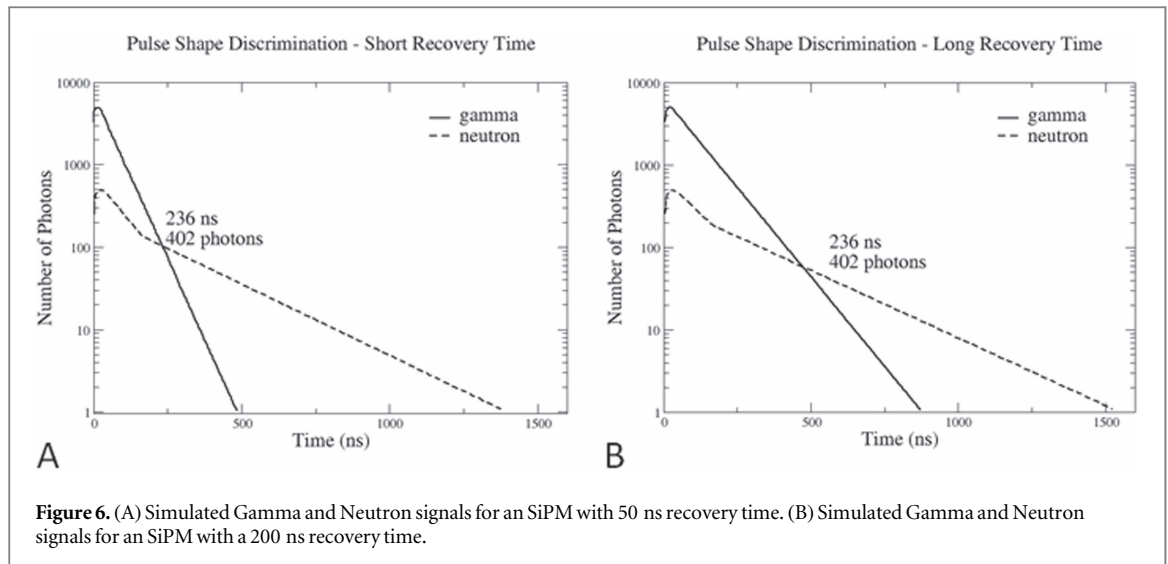
Figure 6 presents simulated curves that emphasize the advantage of the SiPM with short recovery time (6A) over one with a longer recovery time (6B). For the former, the gamma discrimination can be performed after 236 ns compared to 474 ns required for the latter. The short recovery time diode enables a higher rate of measurements. Furthermore, the shorter time periods which are required prior to the discrimination enables higher sensitivity since neutron events with weaker light signal can be detected. The detection of the weak light signal neutron events is made possible by the fact that less of the signal is lost before the discrimination can be performed and the signal remains above the noise level long enough to be detected. At the point where the gamma and neutron decay curves cross, the signal is much higher for the device with the short recovery time than for the one with the longer recovery time (102 photons versus 56).

While using SiPMs with a short recovery time presents a distinct advantage for neutron discrimination, it may be possible to achieve similar results with a device that has a long recovery time but a larger photodetection efficiency. Our analysis indicates that we can boost the signal at the discrimination point to the same as that for the short recovery time device if the PDE of the long recovery time device is 80% higher (see figure 7(A)). This

Table 1. Silicon photomultiplier properties.

Property	Device					
	SensL J-Series 3 mm × 3 mm 35 um	SensL C-Series 3 mm × 3 mm 35 um	Hamamatsu MPPC S12572 3 mm × 3 mm 25 um	EXCELITAS C30742 3 mm × 3 mm 50 um	AdvanSiD RGB3S-P 3 mm × 3 mm 40 um	KETEC sIpm3350 S 3 mm × 3 mm 50 um
Peak wavelength [nm]	420	420	450	<b>470</b>	550	420
Minimal PDE [%] over the light emission range 400 and 530 nm	30, 22	18, 25	32, 34	25, 33	13, 31	<b>35, 40</b>
PDE @470 nm [%]	37	31	35	35	32.5	<b>50</b>
Gain <sup>a</sup>	<b>6 × 10<sup>6</sup></b>	3 × 10 <sup>6</sup>	0.5 × 10 <sup>6</sup>	1.5 × 10 <sup>6</sup>	2.7 × 10 <sup>6</sup>	2 × 10 <sup>6</sup>
Dark Current Rate [MHz]	0.4 Typ. 0.67 Max.	<b>0.3 Typ.</b> <b>0.86 Max.</b>	1 Typ. 2 Max.	1.3 Typ. 2.7 Max.	3.6	4.5
Microcell recovery time [ns]	130	180	25	<b>20<sup>f</sup></b>	220 <sup>f</sup>	N/A
Temperature dependence of V <sub>br</sub> [mV °C <sup>-1</sup> ]	<b>21.5</b>	<b>21.5</b>	60	90	27	N/A
Temperature dependence of Gain [%/°C]	-0.8	-0.8	-1.5	N/A	N/A	N/A
Crosstalk [%]	7	7	13	N/A	32	35
After Pulsing [%]	<b>0.1</b>	0.2	1.5%	N/A	17	N/A
Breakdown voltage tolerance [%]	±10%	±10%	N/A	N/A	N/A	N/A

<sup>a</sup> At manufacturer's recommended operating voltage.



increase can be achieved in matching the peak QE of the device to the output wavelength of the WLS fiber or by increasing the bias voltage. This latter option will work if the corresponding increase in dark noise does not interfere with discrimination. If either of the two analyzed configurations has a lower dark noise rate and lower cross talk it would provide enhanced performance. It is important to note that although these measures can increase the trigger threshold to a robust level, they will not decrease the time required for discrimination.

Another parameter that has a major effect is delayed cross talk. Figure 7(B) shows the same gamma and neutron simulated events presented in figure 7(A) with the addition of 8% delayed cross talk. The delayed cross talk contributes to the tail of the gamma event and therefore the discrimination can only be made after a longer period (302 ns versus 236 ns) and for a lower light amplitude (84 versus 102 photons). For a device with a short recovery time and 8% delayed cross talk, the PDE of the diode with the long recovery time needs to be only 22% higher to obtain a similar sensitivity.

## Pulse shape discrimination

The neutron discrimination method is based on a phenomenon in which the light emission duration (decay time) from a neutron capture event (signal) is longer than the one obtained from a gamma capture or thermal (noise) event. The gamma interaction with the scintillator can produce an event with an amplitude that can be up to twenty times stronger than a neutron capture signal. The opacity of the  ${}^6\text{LiF:ZnS(Ag)}$  scintillator, combined with the short mean free path of the heavy ions, results in a longer decay time for neutron capture events. Our algorithm is based on the ratio between the accumulated signal over the prompt interval (typically

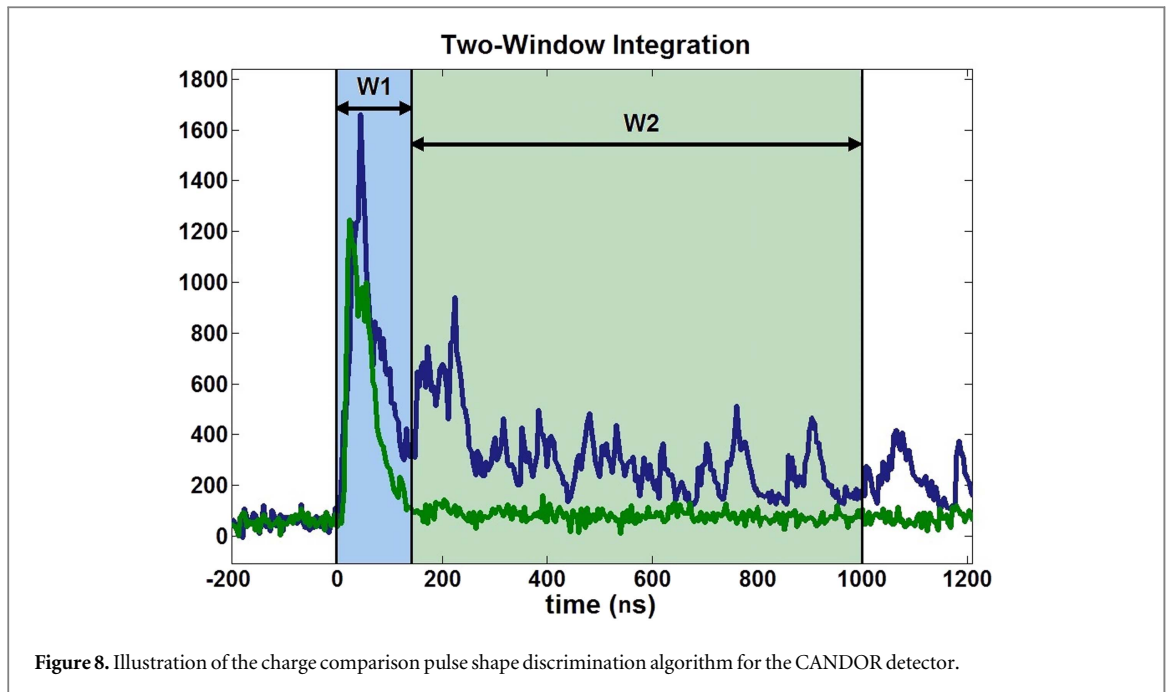


Figure 8. Illustration of the charge comparison pulse shape discrimination algorithm for the CANDOR detector.

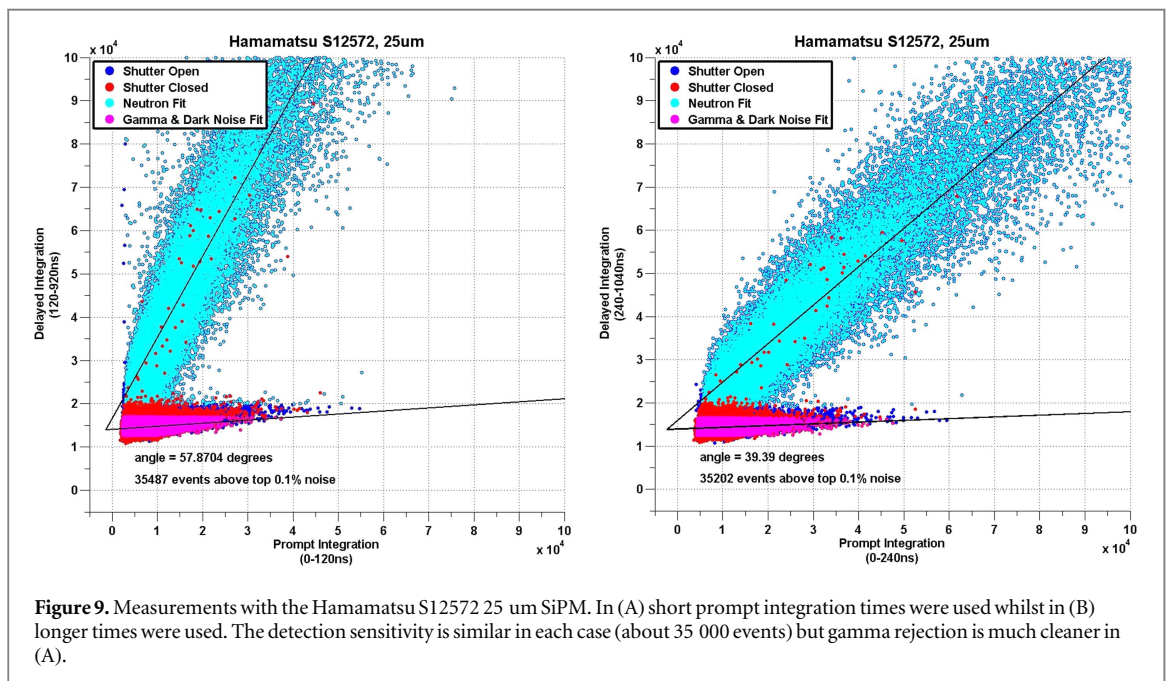
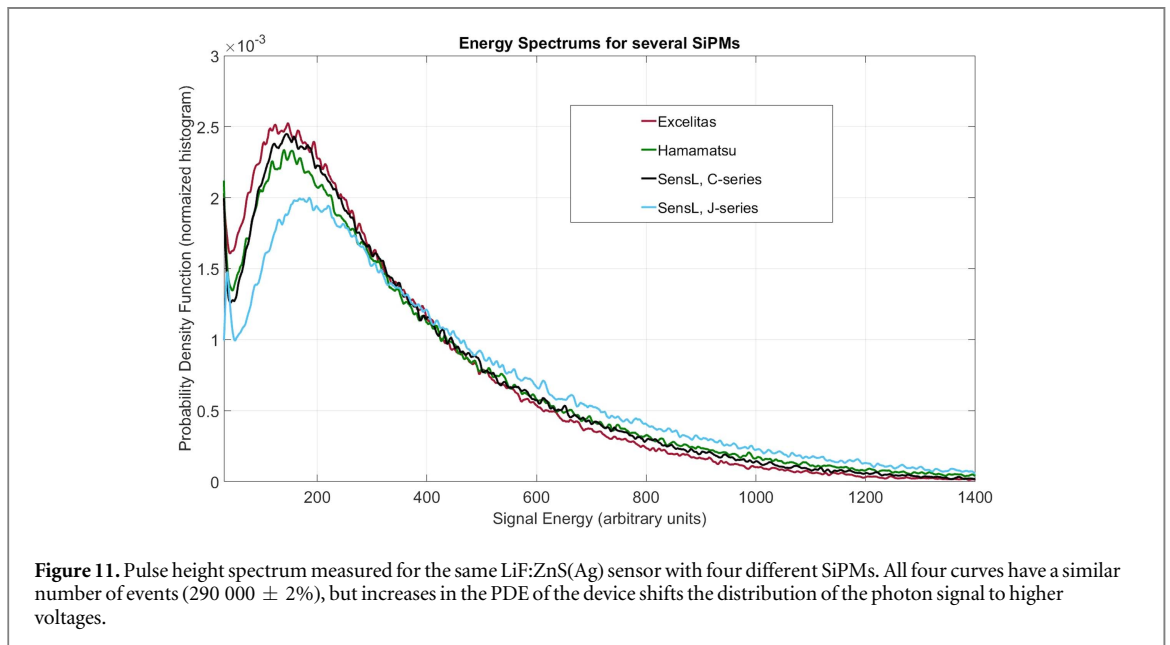
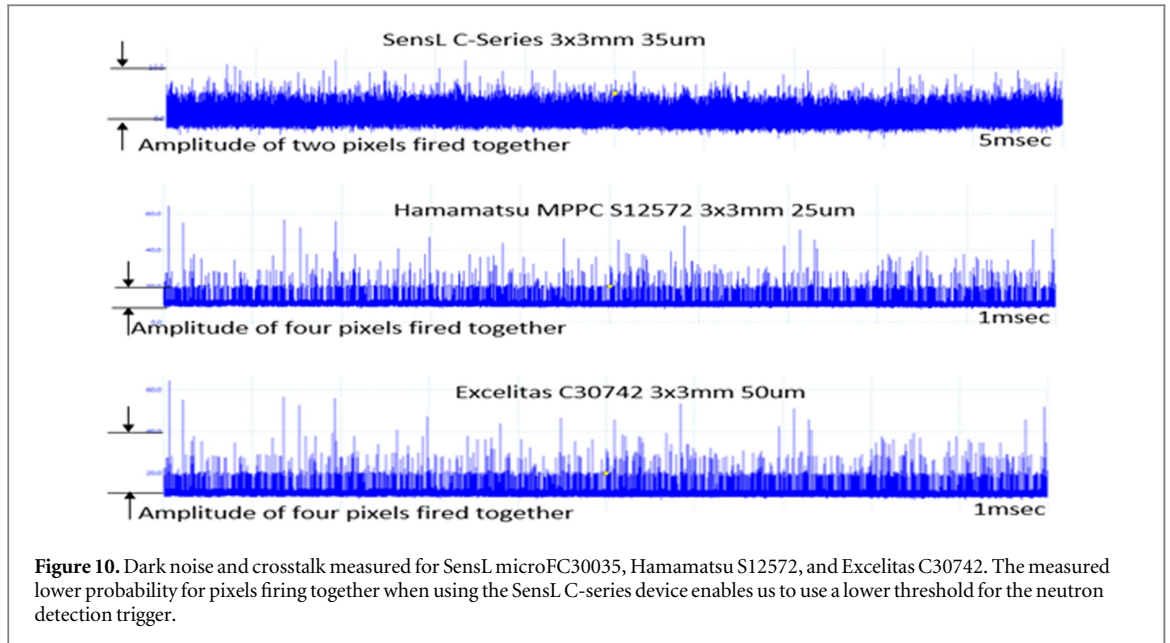


Figure 9. Measurements with the Hamamatsu S12572 25 um SiPM. In (A) short prompt integration times were used whilst in (B) longer times were used. The detection sensitivity is similar in each case (about 35 000 events) but gamma rejection is much cleaner in (A).

$\approx 200$  ns from the initial trigger) and the accumulated signal over the delayed interval (typically  $> 800$  ns) (see figure 8).

Our simulation demonstrated that SiPMs with long recovery times require longer prompt periods for effective discrimination. In figure 6, we demonstrate that for devices with short recovery times it is possible to set higher thresholds for discrimination while simultaneously reducing the prompt integration period.

This can be seen empirically as well. We captured waveforms (as described in the Experimental section above) obtained in mostly gamma fields (closed shutter blocking the neutron beam) and in those with mixed neutron-gamma fields (open shutter allowing a neutron beam to illuminate the detector as well as background gamma radiation). The scatter plots in figure 9 were obtained by mapping events discriminated using short prompt periods (120 ns) and those discriminated using longer prompt periods (240 ns). The duration of the delayed period is 800 ns. Events captured with the shutter closed are colored pink while those captured with the shutter open are blue. A line drawn through the distribution of neutron events has a steeper slope in the case of the shorter prompt integration (57 deg versus 39 deg). This steeper slope presents a cleaner separation of the cloud of neutron events from those which we believe to be largely gamma capture events.



Because they contribute to both the prompt and delayed integrals, thermal noise frequency and crosstalk probability should be considered as factors in SiPM selection. We measured the dark noise of the Hamamatsu S12572  $3\text{ mm} \times 3\text{ mm}$   $35\text{ }\mu\text{m}$  diode and the Excelitas C30742 which both have a short (40 ns) recovery time. We also measured the dark noise of the SensL C-Series 30 035  $3\text{ mm} \times 3\text{ mm}$  with  $35\text{ }\mu\text{m}$  pixels which has a longer (180 ns) recovery time. For the recommended overvoltage, the dark noise of the SensL device was much lower. The diode thermal noise rate and number of events with amplitudes corresponding to four pixels firing together were measured over an interval of 100 msec. The Hamamatsu device had an average of 10 pixels firing together over a period of 1 ms and the Excelitas diode had an average of 410 pixels firing together over that same interval. The measured results are presented in figure 10.

We measured the light yield of the SensL microFJ 30 035, SensL microFC 30 035, Hamamatsu MPPC S12572, and Excelitas C30742 diodes with the same  ${}^6\text{LiF:ZnS(Ag)}$  scintillator (figure 11). All diodes have an active area of  $3\text{ mm} \times 3\text{ mm}$ . The spectra presented in the figure have a similar number of events ( $290\,000 \pm 2\%$ ) for all four diodes. The figure demonstrates the effect of the PDE on the spectra, in that higher PDE shifts the spectrum to higher voltages. SensL's 'J' series diode has the best light spectrum meaning that there is a smaller number of events with low light yield.

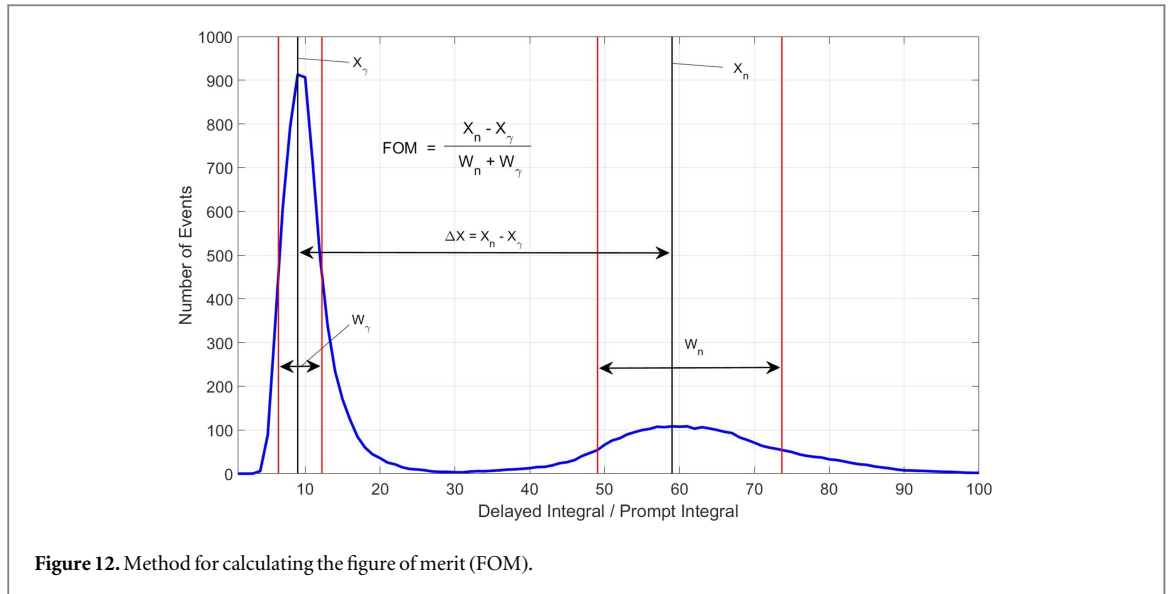


**Table 2.** SensL microFJ 30 035 calculated FOM for operation voltage of 27.1 V, total pulse duration of 0.6, 0.8, 1, 1.2 and 1.5 and prompt integration time of 80, 120, 160, 200 and 240 ns.

Prompt Total	80 ns	120 ns	160 ns	200 ns
600 ns	2.02	2.10	2.14	2.13
800 ns	2.13	2.10	2.05	1.97
1000 ns	2.09	2.11	2.02	1.93
1200 ns	2.11	2.07	2.02	1.92
1500 ns	2.07	2.01	1.93	1.80
2000 ns	2.00	1.94	1.77	1.63

The PDE can be improved by applying a higher bias voltage but this does not necessarily result in improved neutron detection sensitivity. Under these circumstances, signals from gamma rays are also correspondingly larger and this in combination with an increased rate of thermal events and probability of crosstalk may result in false positive events.

To define the optimal operating voltage for achieving the best sensitivity with high gamma rejection we had to define the integration time for prompt and delay periods. Our investigation was based on a figure of merit (FOM) which determines the best gamma rejection. The FOM is calculated from the histogram of the ratio of the integrated signal during the delayed period divided by the integrated signal during the prompt time period, as shown in figure 12 and equation (1) [35, 36] where  $(X_n - X_\gamma)$  is the distance between the gamma event peak and the neutron event peak,  $W_\gamma$  is the Full Width Half Max (FWHM) of the gamma events, and  $W_n$  is the FWHM of the neutron events.

$$FOM = \frac{X_n - X_\gamma}{W_n + W_\gamma} \quad (1)$$

We investigated five time periods for total pulse durations of 0.8  $\mu$ s, 1  $\mu$ s, 1.2  $\mu$ s, 1.5  $\mu$ s, and 2  $\mu$ s. These time intervals were selected to determine the optimal pulse duration permitting good gamma rejection with minimal time overhead associated with discrimination. This analysis was conducted for the SensL microFC 30 035 and the SensL microFJ 30 035 devices. The recovery time for these devices is slightly different (130 ns for microFJ and 180 ns for the microFC). We used prompt integration times of 80 ns, 120 ns, 160 ns, 200 ns, and 240 ns. The shortest prompt integration time (80 ns) was used only for the microFJ and the longest prompt integration time (240 ns) was used only for the microFC. The results were compared using the figure of merit (FOM) calculated per equation (1) and summarized in table 2 for the SensL microFJ 30 035 device and table 3 for the SensL microFC 30 035 device. The trigger for event processing was set to ten photoelectrons (10 pixels fired together). The results on both tables are based on about 10 000 gamma events and about 1000 neutron events at a bias voltage of 27.1 V (2.5 V over breakdown).

The optimal durations for SensL microFJ 30 035 device were determined to be 120 ns for the prompt interval and 1000 ns for the total integration time. The calculated FOM for these parameters was 2.11. Another set of

**Table 3.** MicroFC 30 035 calculated FOM for operation voltage of 27.1 V, total pulse duration of 0.6, 0.8, 1, 1.2 and 1.5  $\mu$ sec and prompt integration time of 80, 120, 160, 200 and 240 ns.

Prompt Total	120 ns	160 ns	200 ns	240 ns
800 ns	1.97	2.04	2.05	2.04
1000 ns	1.95	1.99	1.93	1.91
1200 ns	1.96	1.99	1.95	1.92
1500 ns	1.85	1.78	1.71	1.65
2000 ns	1.69	1.61	1.54	1.47

parameters can yield a higher FOM (as shown in the table for 160 ns prompt and 600 ns delayed) but the selected values are in a more stable region in the phase space. The calculated FOMs shown in table 2 imply that by selecting this FOM as our reference value any error associated with the initial trigger or integration times of the prompt and delayed intervals yields only a small change (less than 5%) for the calculated FOM.

The optimal durations for SensL microFC 30 035 device were determined to be 160 ns for the prompt interval (slightly longer than for the microFJ) and 1000 ns for the total integration time. The calculated FOM for this device was 1.99.

Using bias voltages over the nominal breakdown voltage increases both the PDE and the associated thermal noise, so an additional study is required to determine the optimal bias voltage. The device recovery time does not change as a function of the applied voltage bias so the interval adjustment study was repeated for bias voltages of 28.4 V and 29.6 V. The FOM for the SensL microFC 30 035 device as function of the applied voltage was investigated as well (table 3).

It should be noted that when the bias voltage is increased, the trigger threshold should also be increased. Per the manufacturer's data, which were also validated by our measurements, a fired pixel amplitude increases by 50% when a bias voltage of 28.4 V is applied and by 100% when a bias voltage of 29.6 V is applied so the trigger level of ten photoelectrons were set accordingly. For the selected total pulse duration of 1000 ns and prompt integration time of 160 ns the FOM is found to be 2.11 for 28.4 V and 2.05 for 29.6 V.

## Summary

We have developed an ultrathin detector for cold neutrons. The detector is based on a slab of  $^6\text{LiF:ZnS(Ag)}$  scintillator with embedded wavelength shifting fibers and a silicon photomultiplier (SiPM) used as the photosensor. We have evaluated the most important characteristics of these photosensors to optimize pulse shape neutron/gamma discrimination for both neutron sensitivity and gamma rejection.

SiPMs that are currently commercially available can offer a recovery time of 35 ns, a PDE greater than 35%, a dark noise less than 300 kHz (for devices of 3 mm  $\times$  3 mm active area at ambient temperatures), and a crosstalk of a few percent. Unfortunately, no single device yet combines these desirable characteristics in one package.

The selection process included studies of dark noise, crosstalk, and PDE as functions of bias voltage and operating temperature. We have analyzed the tradeoffs between the parameters and determined the optimal configuration for the CANDoR project.

Over the course of our detector development, SiPM technology has continued to advance and improve, so we can only expect even better matches to our application in the near future. At present, the performance of our sensor for cold neutrons is on par with  $^3\text{He}$  gas filled proportional counters but in a significantly more compact package.

## Disclaimer

Certain trade names and company products are identified to adequately specify the experimental procedure. In no case does such identification imply recommendation or endorsement by the National Institute of Standards and Technology, nor does it imply that the products are necessarily the best for the purpose.

## ORCID iDs

N C Maliszewskyj  <https://orcid.org/0000-0002-5156-7870>

## References

- [1] Goldman A I 2012 Neutron Techniques Introduction *Characterization of Materials* (New York: Wiley)
- [2] Majkrzak C F 'CANDOR Spectrometer,' [Online]. Available: (<http://ncnr.nist.gov/equipment/msnew/ncnr/candor.html>)
- [3] Kuraray, Japan, 'Y-11 Wavelength Shifting Fiber,' [Online]. Available: (<http://kuraray.com/products/plastic/psf.html>)
- [4] Dolgoshein B 2006 Status report on silicon photomultiplier development and its applications *Nucl. Inst. and Meth. A* **563** 368–76
- [5] Ginzburg D, Kopeika N and Paran J 2011 Optimization design fo silicon photomultiplier based radiation detector *Nucl. Inst. and Meth. A* **652** 474–8
- [6] Hutchinson D P, Richards R K and Holcomb D E 1999 Position sensitive neutron detectors using a crossed fiber readout array *Proc SPIE* vol 3769, 88–91
- [7] Rhodes N J 2012 Scintillation detectors *Neutron News* **12** 26–30
- [8] Mosset J-B, Stoykov A, Davydov V, Hildebrandt M, Van Swygenhoven H and Wagner W 2014 Upgrade of the POLDI diffractometer with a ZnS(Ag)/<sup>6</sup>LiF scintillation detector read out with WLS fibers coupled to SiPMs *Journal of Physics: Conference Series* **528** 1–8
- [9] Osovizky A, Pritchard K, Yehuda-Zada Y, Ziegler J, Binkley E, Tsai P, Thompson A, Hadad N, Jackson M, Hurlbut C, Baltic G M, Majkrzak C F and Maliszewskij N C 2018 Design of an ultrathin cold neutron detector *Nucl. Inst. and Meth A* **893** 1–9
- [10] Eljen Technology, 'Thermal Neutron Detector EJ-426,' [Online]. Available: (<http://eljentechnology.com/products/neutron-detectors/ej-426>)
- [11] Van Eijk C W E, Bessiere A and Dorenbos P 2004 Inorganic thermal neutron scintillators *Nucl. Inst. and Meth. A* **529** 260–7
- [12] Litvin V S, Beyaev A D and Ignatov S M 2009 ZnS(Ag)/<sup>6</sup>LiF and LiI(Eu) scintillaotrs and silicon photomultipliers for thermal neutron Dete3ctors with high space and time resolution *Bulletin of the Russian Academy of Sciences: Physics* **73** 219–21
- [13] Mc Gregor D S, Hammin M D, Yang Y H, Gersh H K and Klann R T 2003 Design considerations for thin film coated semiconductor thermal neutron detectors *Nucl. Inst. and Meth. A* **500** 272–308
- [14] Litvin V S, Marin V N, Karaevsky S K, Trunov D N, Axenov S N, Stolyarov A A and Sadykov R A 2016 Scintillation neutron detectors based on solid state photomultipliers and lightguides *Crystallography Reports* **61** 106–10
- [15] Golovin V and Saveliev V 2004 Novel type of avalanche photodetector with geiger mode operation *Nucl. Inst. and Meth. A* **518** 560–4
- [16] Heering A, Musienko Y, Ruchti R, Wayne M, Karneyeu A and Postoev V 2015 Effects of very high radiation on SiPMs *Nucl. Inst. and Meth. A* **824** 111–4
- [17] Andreotti M, Baldini W and Calabrese R 2014 Study of the radiation damage of silicon photomultipliers at the GELINA facility *J. Instrum.* **9** P04004
- [18] Stoykov A, Mosset J-B, Greuter U, Hildebrandt M and Schlumpf N 2015 'A SiPM-based <sup>6</sup>LiF:ZnS scintillation neutron detector *Nucl. Inst. and Meth. A* **787** 361–6
- [19] Mosset J-B, Stoykov A, Greuter U, Hildebrandt M and Schlumpf N 2016 Digital signal processing for a thermal neutron detector using ZnS(Ag): <sup>6</sup>LiF scintillating layers read out with WLS fibers and SiPMs *Nucl. Inst. and Meth.* **824** 319–22
- [20] Hamamatsu, Japan, 'MPPC and MPPC modules for precision measurement,' [Online]. Available: ([http://hamamatsu.com/resources/pdf/ssd/mppc\\_kapd0004e.pdf](http://hamamatsu.com/resources/pdf/ssd/mppc_kapd0004e.pdf))
- [21] Bailey G M and Prescott J R 1958 Decay time of the luminescence of a zinc sulphide neutron detector fro neutron and gamma ray excitation *Australian Journal of Physics* **11** 135–8
- [22] Tsunesaboro A, Masayoshi M and Masayuki O 1959 Decay properties of ZnS(Ag) phosphors *J. Phys. Soc. Japan* **14** 1766–70
- [23] Katagiri M, Sakasai K and Masubayashi M 2004 Neutron/gamma ray discrimination characteristics of novel neutron scintillators *Nucl. Inst. and Meth. A* **529** 317–20
- [24] Chong W, Tang B, Sun Z, Luo W and Wang T 2013 The Monte Carlo simulation on a scintillator neutron detector *Science China Physics* **56** 1892–6
- [25] Para A 'Afterpulsing in Silicon Photomultipliers: impact on the Photodetectors Characterization,' [Online]. Available: (<https://arxiv.org/abs/1503.01525>)
- [26] Rosado J and Hidalgo S 2015 Characterization and modelling of crosstalk and afterpulsing in hamamatsu silicon photomultipliers *J. Instrum.* **10** P10031
- [27] AdvanSiD, Italy, 'NUV SiPMs,' [Online]. Available: ([http://advansid.com/attachment/get/up\\_93\\_1432733135.pdf](http://advansid.com/attachment/get/up_93_1432733135.pdf))
- [28] AdvanSiD, Italy, 'RGB SiPMs,' [Online]. Available: ([http://advansid.com/attachment/get/up\\_93\\_1433424300.pdf](http://advansid.com/attachment/get/up_93_1433424300.pdf))
- [29] SensL, Ireland, 'B-Series,' [Online]. Available: (<http://sensl.com/downloads/ds/DS-MicroBseries.pdf>)
- [30] SensL, Ireland, 'C-Series,' [Online]. Available: (<http://sensl.com/downloads/ds/DS-MicroCseries.pdf>)
- [31] SensL, Ireland, 'J-Series Family,' [Online]. Available: (<http://sensl.com/products/j-series/>)
- [32] Collazuol G 'SiPM Behavior at Low Temperatures,' [Online]. Available: (<http://bo.infn.it/sm/sm10/presentations/s20/g-collazuol.pdf>)
- [33] Dinu N, Nagai A and Para A 2017 Breakdown voltage and triggering probability of SiPM from IV curves at different temperatures *Nucl. Inst. and Meth. A* **845** 64–8
- [34] Mikhailik V B, Henry S and Horn M 2013 Investigation of the luminescence and scintillation properties of ZnS(Ag)/<sup>6</sup>LiF in the 7–295 K temperature range *J. Lumin.* **134** 63–6
- [35] Knoll G F 1999 *Radiation Detection and Measurement* (New York: Wiley)
- [36] Pino F, Stevanato L, Cester D, Nebbia G, Sujo-Bolius L and Viesti G 2015 Study of the thermal neutron detector ZnS(Ag)/LiF response using digital pulse processing *J. Instrum.* **10** T08005